

Achieving steady-state Bose-Einstein condensation

J. Williams, R. Walser, C. Wieman, J. Cooper, and M. Holland
JILA and Department of Physics, University of Colorado, Boulder, Colorado 80309-0440
 (Received 7 October 1997)

We investigate the possibility of obtaining Bose-Einstein condensation (BEC) in a steady state by continuously loading atoms into a magnetic trap while keeping the frequency of the radio frequency field fixed. A steady state is obtained when the gain of atoms due to loading is balanced with the three dominant loss mechanisms due to elastic collisions with hot atoms from the background gas, inelastic three-body collisions, and evaporation. We describe our model of this system and present results of calculations of the peak phase-space density ρ_0 in order to investigate the conditions under which one can reach the regime $\rho_0 \geq 2.612$ and attain BEC in steady state. [S1050-2947(98)05503-6]

PACS number(s): 03.75.Fi, 05.20.Dd, 32.80.Pj

I. INTRODUCTION

In the usual method of evaporative cooling used so far in Bose-Einstein condensation (BEC) experiments [1–6], a finite number of atoms are collected in a magnetic trap after being laser cooled to a phase space density at least five orders of magnitude below the critical density needed for BEC. The frequency of an external RF radiation field, which spin-flips the atoms to an untrapped state, is then lowered continuously. This further cools the gas by removing high energy atoms from the tail of the distribution. This evaporative cooling procedure increases the phase space density above the critical point needed to reach BEC. The success of this method is well established experimentally, allowing many fundamental properties of Bose-Einstein condensation to be investigated [7–12].

This standard method of achieving BEC has one critical drawback: once a condensate has been obtained, it has a finite lifetime in the trap determined by various loss mechanisms, such as collisions with hot atoms from the background gas, and inelastic collisions between the trapped atoms. Although the finite lifetime of the condensate does not prevent many crucial properties of the system to be studied, it is still very desirable to achieve a steady-state situation so that a condensate can be sustained for an indefinite period of time. Such a situation is essential for the continuous output of a coherent beam of atoms in an atom laser [13–18]. To date, no experiment has demonstrated a steady-state condensation.

We address this problem by constructing an intuitive model describing the two aspects to such an experiment: The continuous loading of atoms into the magnetic trap and the classical kinetic evolution of the trapped atoms toward a steady state during the evaporation. Our description of the loading procedure is based on the experimental setup described in [19], where the authors loaded a magnetic trap with atoms which had been cooled in a separate MOT. This allows us to estimate the rate γ_f that atoms enter the trap below the RF cut, as well as the mean energy e_f of the injected atoms.

To model the classical kinetic evolution, we assume a truncated Boltzmann distribution for the trapped atoms and obtain rate equations for the total number $N(t)$ and energy

$E(t)$ of the system [1,3–6]. These rate equations include the loss of atoms due to elastic collisions with the background-gas atoms, inelastic three-body collisions, and evaporation, as well as the gain of atoms due to loading. We then numerically calculate the steady-state solution of these equations and show plots of the peak phase space density ρ_0 as a function of the various physical parameters of the system. We show that the critical regime $\rho_0 \geq 2.612$ may be reached in order to obtain BEC in steady state.

II. DESCRIPTION OF THE MODEL

In constructing a model of steady-state evaporative cooling, there are several experimental schemes one could consider for describing the loading of atoms into the magnetic trap, as well as several layers of approximation in describing the kinetic evolution of the trapped gas toward steady state. However, we consider only one realization of the loading procedure, assuming the atoms are first trapped and cooled in a MOT and then transferred to a separate magnetic trap [19,20,11]. Furthermore, we consider a simplified model of evaporative cooling that assumes classical statistics, and is therefore valid only for phase space densities below the critical point $\rho_0 = 2.612$; one would have to include quantum statistics in order to properly model the system above this point. These two parts to our model are described in the following subsections.

A. Description of the loading procedure

In a real experiment, irreversibility is introduced at each step of the transfer of the atoms from the MOT to the magnetic trap; the atoms are first pushed out of the MOT, they then travel through a magnetically confining tube, and finally must be caught in the magnetic trap and optically pumped into a trapped hyperfine state. In order not to get lost in the details of modeling all of these heating and loss mechanisms, we consider two extreme idealizations of the transfer: an adiabatic transfer which preserves the phase space density ρ_0 and a sudden, irreversible transfer which decreases ρ_0 .

We assume the atoms feel an isotropic, linear restoring force in both the MOT and the magnetic trap, neglecting the possibility of a radiation pressure in the MOT, which would

distort the effective harmonic trapping potential [21]. Then the free Hamiltonian of an atom in either trap can be written

$$H_i(r,p) = \frac{p^2}{2m} + \frac{1}{2}m\omega_i^2 r^2, \quad (1)$$

where m is the mass of the atom, and ω_i is the effective radial frequency of the trapping potential. The index $i=1$ indicates the MOT, while $i=2$ indicates the magnetic trap.

We model the transfer of atoms in order to obtain a reasonable estimate of the feed rate γ_f and the mean energy e_f of atoms injected into the trap below the RF cut. We treat this transfer process as a succession of discrete transfers each consisting of a finite number of atoms. We only need to consider a snapshot of this transfer process: a finite number of atoms N_1 are collected in the MOT at a temperature T_1 in equilibrium, they are then either adiabatically or suddenly transferred to the magnetic trap. In our model, we allow these N_1 atoms to come to an equilibrium in the magnetic trap, characterized by a new temperature T_2 . We then place the RF cut e_{cut} and calculate the fraction of atoms α_f which remain in the magnetic trap below e_{cut} , as well as the mean energy per atom e_f of these atoms,

$$\alpha_f = \frac{\int_0^{e_{\text{cut}}} e^2 e^{-e/k_B T_2} de}{\int_0^{\infty} e^2 e^{-e/k_B T_2} de}, \quad (2)$$

$$e_f = \frac{\int_0^{e_{\text{cut}}} e^3 e^{-e/k_B T_2} de}{\int_0^{e_{\text{cut}}} e^2 e^{-e/k_B T_2} de}. \quad (3)$$

The e^2 factor appears due to the density of states for an isotropic harmonic oscillator potential. A schematic diagram in Fig. 1 illustrates the transfer process.

This process can be repeated many times each second so that atoms are transferred to the magnetic trap at a rate γ_t . The rate that atoms enter below the RF threshold e_{cut} is then given by $\gamma_f = \alpha_f \gamma_t$. We estimate an upper limit on the number of these transfers each second to be on the order of 100.

The equilibrium temperature T_2 which the atoms attain after a sudden transfer can be obtained by considering the sudden change in the energy of the atoms after the instantaneous change in trapping frequencies $\omega_1 \rightarrow \omega_2$. Then for a sudden transfer, the temperature T_2 is related to the temperature T_1 in the MOT according to

$$T_2 = \frac{T_1}{2} \left(1 + \frac{\omega_2^2}{\omega_1^2} \right) \quad (\text{sudden}). \quad (4)$$

The adiabatic case can be treated as a succession of infinitesimal steps $\omega_1 \rightarrow \omega_1 + \delta\omega$, each treated as a sudden transfer. This yields the relationship

$$T_2 = T_1 \frac{\omega_2}{\omega_1} \quad (\text{adiabatic}). \quad (5)$$

Note that both cases give $T_2 = T_1$ when $\omega_2 = \omega_1$ as they must. With the peak phase space density $\rho_0 = n_0 \Lambda^3$ of the trapped atoms given by

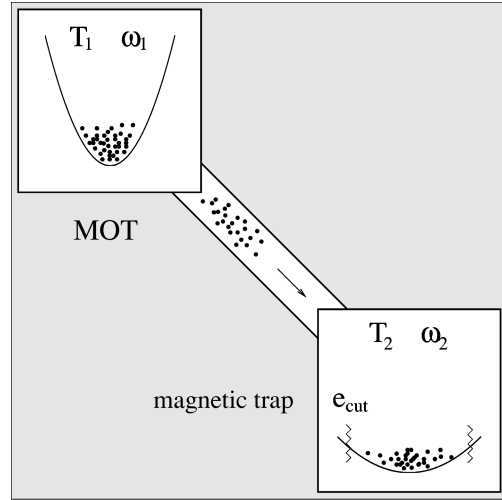


FIG. 1. This diagram illustrates the transfer process described in Sec. II A. A finite number of atoms are cooled in the MOT to a temperature T_1 in equilibrium. We approximate the potential in the MOT as an isotropic harmonic oscillator at frequency ω_1 . They are then transferred to the magnetic trap, either suddenly, or adiabatically. We also approximate the magnetic trap as forming an isotropic harmonic oscillator potential, with a different frequency ω_2 . In equilibrium, the atoms have a temperature T_2 in the magnetic trap. Then, the RF energy threshold e_{cut} is applied and only a portion of the original atoms from the MOT remains. This transfer can be repeated many times in order to obtain a piecewise continuous transfer of atoms.

$$\rho_0 = N_1 \left(\frac{\hbar \omega_i}{k_B T_i} \right)^3, \quad (6)$$

it is clear that ρ_0 is invariant through an adiabatic transfer, while it decreases after a sudden transfer. Here, Λ is the de Broglie wavelength and n_0 is the peak spatial density.

The two quantities γ_f and e_f depend on the frequency in the lower trap ω_2 , as well as the RF field threshold e_{cut} ; as the trap is made looser, more atoms will make it into the trap below the cut so that γ_f increases. The feed rate is also increased as e_{cut} is raised, however the mean energy e_f of those atoms increases as well.

B. Description of evaporative cooling

With the feeding rate γ_f and mean energy per atom e_f of the injected atoms given by the above model of the loading procedure, it remains to describe the kinetic evolution of the atoms in the magnetic trap during evaporation. Our model can be constructed on phenomenological considerations, with the goal of characterizing the steady state of the system.

We characterize the trapped atoms by a single-particle distribution over energy $\rho(e)f(e,t)$ instead of retaining the more detailed description in phase space using $f(\vec{x}, \vec{p}, t)$ [1]. Here $\rho(e)$ is the density of states for an isotropic harmonic potential. We also make an assumption that the nonequilibrium distribution $f(e,t)$ of the system can be well approximated by a truncated Boltzmann distribution [1,3–6]

$$f(e,t) = \begin{cases} \eta(t)e^{-\beta(t)e}, & e < e_{\text{cut}} \\ 0, & e \geq e_{\text{cut}}, \end{cases} \quad (7)$$

where $\eta(t)$ and $\beta(t) = 1/k_B T(t)$ are functions of time. They are related to the total number $N(t)$ and total energy $E(t)$ of the atoms according to

$$N(t) = \int_0^{e_{\text{cut}}} de \rho(e) f(e,t), \quad (8)$$

$$E(t) = \int_0^{e_{\text{cut}}} de \rho(e) e f(e,t). \quad (9)$$

With the assumption of the truncated Boltzmann form for $f(e,t)$, the description of the system can be reduced to finding the equations of motion for the total number and energy.

The equations of motion for $N(t)$ and $E(t)$ will be written in terms of the various gain and loss processes which occur. There are four competing processes which take place during the evaporation: the constant feeding of atoms into the trap at a rate γ_f with a mean energy per atom e_f , the loss of atoms from the trap due to collisions with the atoms from the hot background gas, characterized by a constant rate γ_{bl} , the loss of atoms and heating due to three-body inelastic collisions, given by the rate γ'_3 , and the rethermalization due to elastic collisions which will eject atoms from the trap which obtain an energy above e_{cut} after a collision. We can include all of these effects in the kinetic equation for $f(e,t)$,

$$\rho(e) \frac{\partial f(e,t)}{\partial \tau} = \gamma_f g_f(e) - \gamma_{\text{bl}} \rho(e) f(e,t) - \gamma'_3 (\rho(e) f(e,t))^3 + \Gamma_{\text{col}}(t), \quad (10)$$

where the distribution of atoms injected into the trap is $g_f(e)$ and the density of states is $\rho(e) = \frac{1}{2} e^2 / (\hbar \omega_2)^3$. $\Gamma_{\text{col}}(t)$ is the collision integral given by [1]

$$\Gamma_{\text{col}}(t) = \gamma_0 \int de_r de' de'_r \delta(e + e_r - e' - e'_r) \rho(e_{\text{min}}) \times [f(e') f(e'_r) - f(e) f(e_r)], \quad (11)$$

where $\gamma_0 = m\sigma / (\pi^2 \hbar^3)$ and $e_{\text{min}} = \min\{e, e_r, e', e'_r\}$ is the minimum energy.

By substituting Eq. (7) into Eq. (10), and using Eq. (8) and Eq. (9), we obtain the following equations of motion for the total number and total energy:

$$\dot{N} = \gamma_f - \gamma_{\text{bl}} N - \gamma_3 N^3 - \Gamma_N, \quad (12)$$

$$\dot{E} = \gamma_f e_f - \gamma_{\text{bl}} E - \frac{2}{3} \gamma_3 N^2 E - \Gamma_E, \quad (13)$$

where the three-body loss rate for the total number is $\gamma_3 = 3^{1.5} K_3 (m \omega_2^2 / 2 \pi k_B T)^3$. K_3 is an experimentally determined constant to be specified [22]. In obtaining the three-body loss terms, an approximation has been made that $e_{\text{cut}} \gg k_B T(t)$ in order to simplify the terms. Initially during the evolution, this assumption may not hold, but the density is low enough that the three-body loss terms are negligible in any case. By the time the density has increased enough so

TABLE I. This is a table showing the values used for the various physical parameters needed in the model. σ_{Rb} is the s -wave scattering cross section for ^{87}Rb . The explanations for the other parameters are given in the text.

σ_{Rb}	$7.5 \times 10^{-16} \text{ m}^2$
$\tau_{\text{bl}} \equiv 1/\gamma_{\text{bl}}$	200 s
K_3	$4.9 \times 10^{-29} \text{ cm}^6/\text{s}$
$T_1^{(\text{ref})}$	20 μK
$\omega_1^{(\text{ref})}/2\pi$	100 Hz
$\gamma_t^{(\text{ref})}$	10^7 atoms/s

that three-body losses are significant, the assumption does hold. The factor of 2/3 in Eq. (13) signifies that the energy will decrease at a slower rate than the number due to three-body losses, which gives rise to an effective heating.

The two terms Γ_N and Γ_E represent the loss of number and energy due to evaporation and are given by

$$\Gamma_N = \gamma_0 \int_0^{e_{\text{cut}}} de \int_{e_{\text{cut}}-e}^{e_{\text{cut}}} de_r \int_0^{e+e_r-e_{\text{cut}}} de'_r \rho(e'_r) f(e,t) f(e_r,t), \quad (14)$$

$$\Gamma_E = \gamma_0 \int_0^{e_{\text{cut}}} de \int_{e_{\text{cut}}-e}^{e_{\text{cut}}} de_r \times \int_0^{e+e_r-e_{\text{cut}}} de'_r e' \rho(e'_r) f(e,t) f(e_r,t). \quad (15)$$

The fourth atom in these equations is lost from the trap since its energy is always greater than the RF cut $e' > e_{\text{cut}}$. Due to energy conservation and the truncated form of $f(e)$, this means that $e_{\text{min}} = e'_r$, as indicated in Eq. (14) and Eq. (15). Also, the energy which appears in the term $\Gamma_E(t)$ is that of the escaping atom $e' = e + e_r - e'_r$.

III. RESULTS

In order to carry out explicit calculations, we choose realistic values of the various physical parameters needed in our model. These are listed in Table I for a gas of ^{87}Rb atoms. The parameters ω_2 and e_{cut} are not listed in the table but are variables to be specified in the following calculations. We have specified a reference point for the MOT parameters which yields a phase space density in the MOT of $\rho_0 = 6.9 \times 10^{-6}$, if one assumes that $N_1 = 5 \times 10^5$ at 20 transfers per second [21].

A. Time evolution

We first consider the dynamical evolution of the system toward steady state. In Fig. 2 we show results of a numerical integration of the rate equations in Eq. (12) and Eq. (13) for the total number $N(t)$ and energy $E(t)$. Since the magnetic trap frequency ω_2 is matched to the MOT frequency ω_1 in this calculation, the adiabatic and sudden transfers are equivalent. For case 1 in the figure, we chose the optimum value of e_{cut} to yield the highest phase space density ρ_0 ,

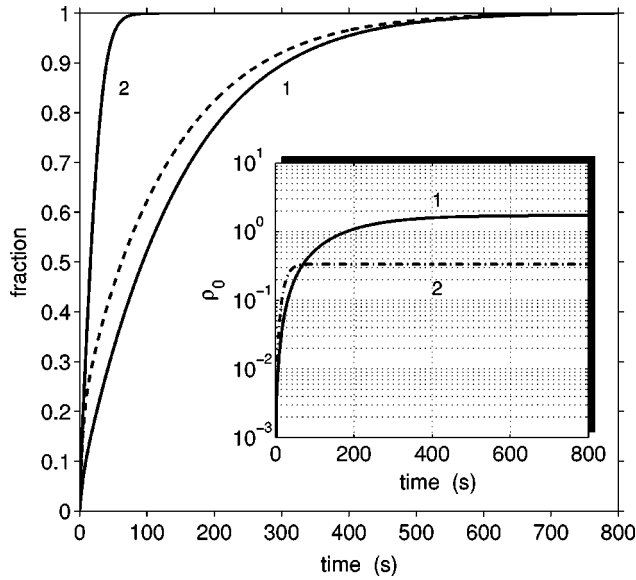


FIG. 2. This plot shows the time evolution of the total number $N(t)$ and total energy $E(t)$ for the values of the parameters listed in Table I. The magnetic trap frequency is equal to the MOT frequency $\omega_2 = \omega_1$ in this calculation. Two values of e_{cut} were chosen: $1.1 \mu\text{K}$, labeled by 1, and $11 \mu\text{K}$, labeled by 2. Each of the curves is normalized by its final steady-state value. The solid curve is the total number and reaches a steady-state value of $N_{\text{ss}} = 2.0 \times 10^4$ for case 1, and $N_{\text{ss}} = 2.8 \times 10^6$ for case 2. The dashed curve is the total energy and reaches a steady-state value of $E_{\text{ss}} = (0.33 \mu\text{K})N_{\text{ss}}$ for case 1 (case 2 is not shown). The evolution of the peak phase space density ρ_0 is shown in the inset for the two cases.

while in case 2 the value chosen for e_{cut} is ten times higher than that in case 1. There are some interesting features to consider from this plot.

It is instructive to take a simple limiting case of Eq. (12) and Eq. (13) in order to learn something about the build-up time for steady state to occur. If we let $e_{\text{cut}} \rightarrow \infty$ and $\gamma_3 = 0$, then the solution to the rate equations for $N(t)$ and $E(t)$ is given by

$$N(t) = \frac{\gamma_t}{\gamma_{\text{bl}}} (1 - e^{-\gamma_{\text{bl}} t}),$$

$$E(t) = \frac{\gamma_t}{\gamma_{\text{bl}}} e_f (1 - e^{-\gamma_{\text{bl}} t}). \quad (16)$$

The time scale for steady state to occur in this simple case is just the lifetime of the trap as determined by background losses, τ_{bl} . In the case where the RF cut is present and evaporation is occurring, while still neglecting three-body losses, the build-up time for steady state will be on the order of magnitude of τ_{bl} , although it will be shorter, based on results of numerical calculations. We define this build-up time to be the time at which $N(t) = (1 - e^{-1})N_{\text{ss}}$. When three-body losses are included, the build-up time can be very short compared to τ_{bl} if the density is high enough for three-body losses to dominate. So this gives us an upper limit of the build-up time to be τ_{bl} , and if steady state occurs on a much shorter time scale than this, it indicates that three-body losses are dominating the other loss mechanisms.

In Fig. 2, the build-up time in case 1 is slightly less than τ_{bl} , which is 200 seconds. This indicates that the choice of e_{cut} in case 1 minimizes three-body losses. In case 2, on the other hand, where e_{cut} is ten times larger than that in case 1, the build-up time is much shorter at roughly 25 seconds. This is because in case 2, γ_f is larger, causing the density to build up more quickly which allows three-body losses to dominate. This also stops the evaporative cooling quickly and so one does not obtain as high of a phase space density ρ_0 as in case 1. It should be noted that when we calculated case 2 with $\gamma_3 = 0$, the build-up time was approximately equal to τ_{bl} , and the steady-state value of the phase space density was close to being optimized at that value of e_{cut} , with $\rho_0 = 3.9$ in steady state.

B. Steady-state solution

Now that we have characterized the time scale for steady state to occur, it is useful to solve Eq. (12) and Eq. (13) directly for the steady-state values of N_{ss} and E_{ss} by setting the left-hand sides equal to zero. We were not able to solve the resulting coupled algebraic equations analytically, since they are transcendental in form. However, they are straightforward to solve numerically. In the following sections, we present calculations of the steady-state value of ρ_0 while varying some of the physical parameters in order to discern what values of the parameters yield $\rho_0 = 2.612$ so that BEC can be achieved in steady state.

1. Varying e_{cut} and ω_2

In trying to understand what it takes to reach a steady-state BEC, it is useful to look at how ρ_0 varies with ω_2 and e_{cut} . In Fig. 3 and Fig. 4, we show shaded contour plots of the steady-state value of ρ_0 , for both an adiabatic and a sudden transfer. Also shown are contours of the total number N_{ss} overlaying the shaded contours. Again, we use the reference point of parameters displayed in Table I. The two different idealizations of the transfer process yield quite distinct shapes for the surfaces of ρ_0 and N_{ss} .

For the adiabatic case shown in Fig. 3, ρ_0 increases with increasing ω_2 , keeping e_{cut} fixed. However, it levels off quite quickly, varying from 1.1 to 1.5 with an order of magnitude increase in ω_2/ω_1 from 0.1 to 1.0 at $e_{\text{cut}} = 1 \mu\text{K}$. Also, with ω_2 fixed, the optimum value of e_{cut} which yields the highest ρ_0 does not depend much on ω_2 , but is roughly a straight line at $e_{\text{cut}} = 1 \mu\text{K}$. Perhaps the most interesting and crucial feature exhibited in the plot is that N_{ss} decreases very rapidly as ω_2 is increased, going from 10^7 down to 10^4 as ω_2/ω_1 goes from 0.1 to 1.0. This is because three-body losses increase as the trap is tightened, since the density increases. Therefore, one will gain a lot in number by keeping the magnetic trap shallow, while losing only a small amount in phase space density.

The results of a sudden transfer are shown in Fig. 4. The most striking difference between this and the plot shown in Fig. 3 for an adiabatic transfer is a strong peak which occurs at $\omega_2/\omega_1 = 1$. This can be attributed to the fact that the phase space density always decreases in a sudden transfer, with a peak occurring at $\omega_2 = \omega_1$, where the sudden and adiabatic transfers are equivalent. Notice also that ρ_0 drops off much more rapidly as ω_2/ω_1 is varied from unity, compared to the

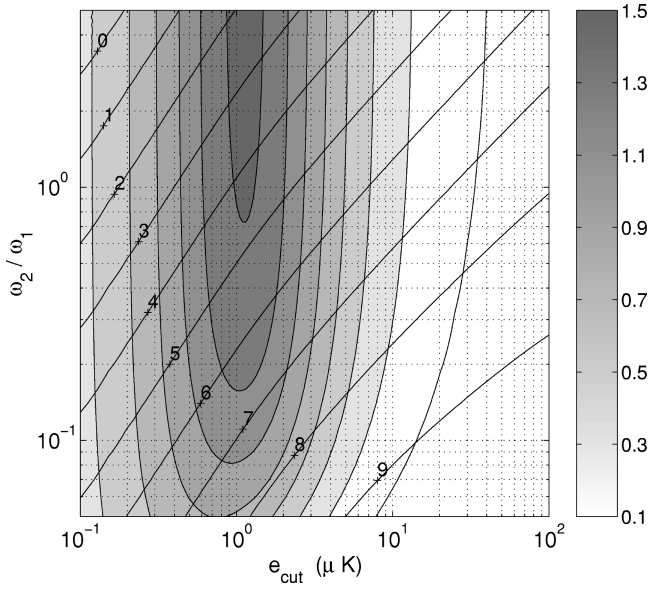


FIG. 3. This plot shows two overlaying contours of the steady-state value of the phase space density and the total number vs the ratio of trap frequencies and RF cut threshold for an adiabatic transfer. The shaded contours represent the steady-state value of ρ_0 , with the gray-scale bar shown to the right. The numbered lines represent $\log_{10}N_{ss}$ (i.e., a value of 6 for the line in the center corresponds to $N_{ss}=10^6$). It is ω_2 that is varied in the ratio, while ω_1 is fixed at $2\pi 100$ Hz. The values used for the other parameters are displayed in Table I.

adiabatic case. Another difference between the two cases is that the optimum value for e_{cut} increases as ω_2/ω_1 is varied from unity. Finally, it can be seen also that one does not gain that much in number as ω_2 is decreased, in sharp contrast to the adiabatic case.

2. Varying T_1 and γ_t

We now have an understanding of how the steady-state values of ρ_0 and N_{ss} vary with e_{cut} and ω_2 . Another useful

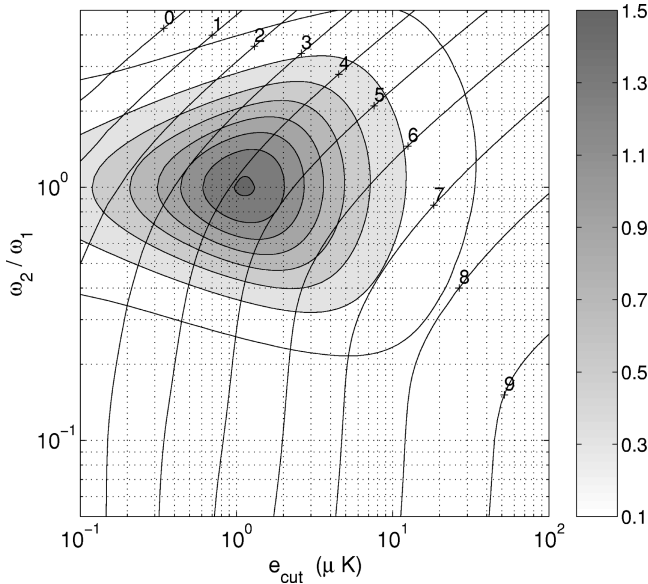


FIG. 4. This plot is the same as described in the caption of Fig. 3 except for a sudden transfer of atoms from the MOT to the magnetic trap, instead of an adiabatic one.

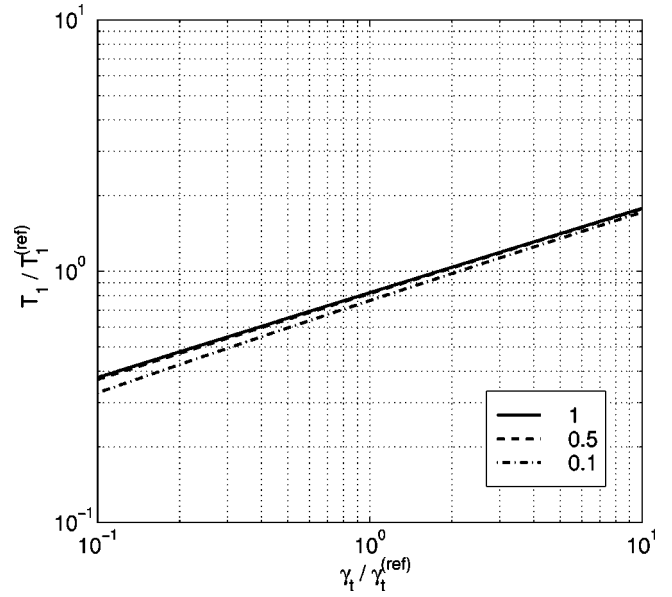


FIG. 5. This plot shows the values of T_1 and ω_2 one must achieve in order to reach $\rho_0=2.612$ in the case of an adiabatic transfer. Three different values of $\omega_2/\omega_1 \in \{0.1, 0.5, 1\}$, with $\omega_1=2\pi \times 100$ Hz. For each line, e_{cut} was chosen so as to maximize ρ_0 . The reference values are $T_1^{(ref)}=20 \mu\text{K}$ and $\gamma_t^{(ref)}=10^7$ atoms/s.

calculation is to see how ρ_0 depends on the MOT temperature T_1 and the transfer rate γ_t . In the plots below, e_{cut} is chosen so as to maximize ρ_0 , for a given T_1 , γ_t , and ω_2 . Then, given γ_t and ω_2 , T_1 is chosen so as to reach $\rho_0=2.612$. This is done for $10^6 \leq \gamma_t \leq 10^8$, as well as three values of the trap frequency ratio $\omega_2/\omega_1 \in \{0.1, 0.5, 1\}$, with $\omega_1=2\pi \times 100$ Hz.

The results of an adiabatic transfer are shown in Fig. 5. Along each of the three lines $\rho_0=2.612$. The most important feature of this plot is that the three lines lie nearly on top of each other. This agrees with Fig. 3 in that ρ_0 decreases very little as ω_2 is lowered. The plot also shows that ρ_0 depends more critically on T_1 than on γ_t . Starting from the reference point in the center, one has to either decrease T_1 by 20%, or increase γ_t by 100% in order to get to the $\rho_0=2.612$ line.

The sudden transfer is shown in Fig. 6. In contrast to the adiabatic case, the three lines are separated, so that as ω_2 is decreased, one has to try much harder to reach $\rho_0=2.612$, which is also consistent with Fig. 4.

The N_{ss} curves corresponding to the $\rho_0=2.612$ lines in Fig. 5 and Fig. 6 are shown in Fig. 7. The results are the same in both the sudden and adiabatic cases (thus there are only three lines instead of six). For the adiabatic case, by loosening the magnetic trap, one does not have to vary T_1 and γ_t much at all in order to stay at $\rho_0=2.612$ while increasing the number N_{ss} by orders of magnitude. On the other hand, for the sudden transfer, one has to decrease T_1 and increase γ_t a lot in order to stay at $\rho_0=2.612$ as ω_2 is decreased. However, one will achieve the same increase in number as in the adiabatic case.

Finally, in Fig. 8 we show a plot of the ratio e_{cut}/T_2 corresponding to the $\rho_0=2.612$ lines shown in Figs. 5–7. This ratio of the optimum cut to the temperature T_2 of atoms being injected into the trap is the same in both the adiabatic

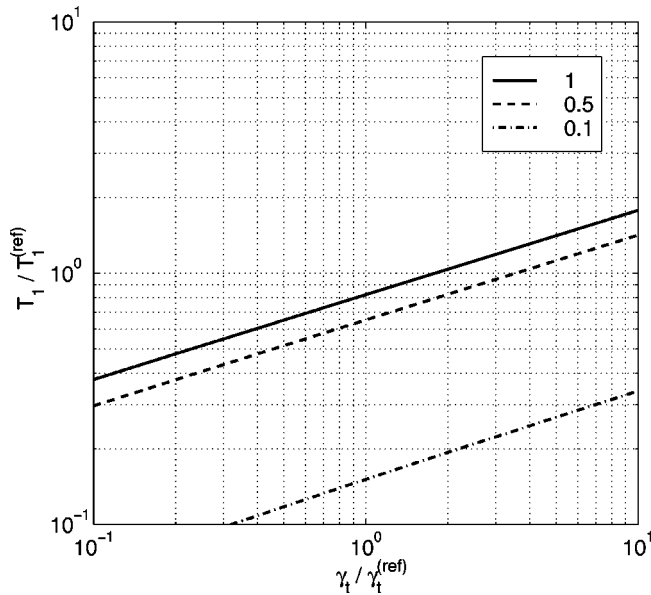


FIG. 6. This plot is the same as described in the caption of Fig. 5 but for the case of a sudden transfer.

and sudden transfers. As ω_2 is decreased, one does not have to exclude as much of the distribution from the trap. Also, as γ_t is increased, one has to cut further into the injected distribution in order to prevent three-body losses from dominating.

IV. CONCLUSION

In this paper we have addressed the problem of achieving a steady-state condensation by continuously feeding atoms into the magnetic trap below a fixed RF threshold. We have included losses due to elastic collisions with atoms from the

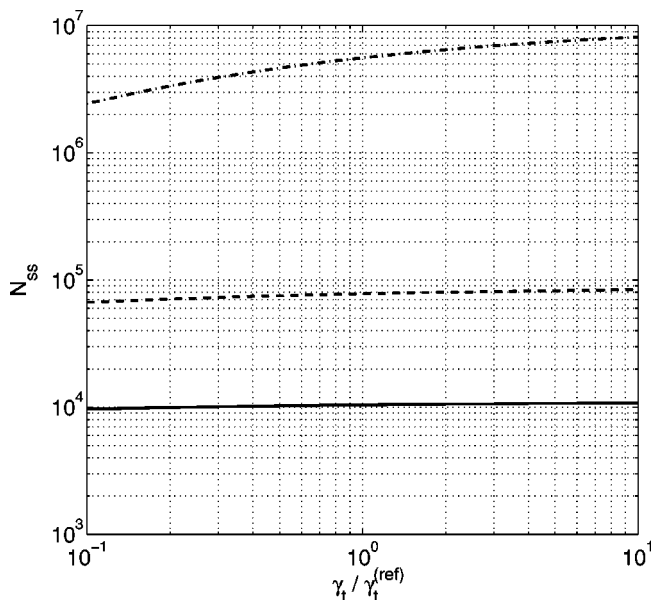


FIG. 7. This plot corresponds to the three lines in both Fig. 5 and Fig. 6, showing the total number of atoms in steady state N_{ss} as a function of the transfer rate γ_t . Along each of these curves, $\rho_0=2.612$. The legend in Fig. 5 and Fig. 6 applies to this plot also.

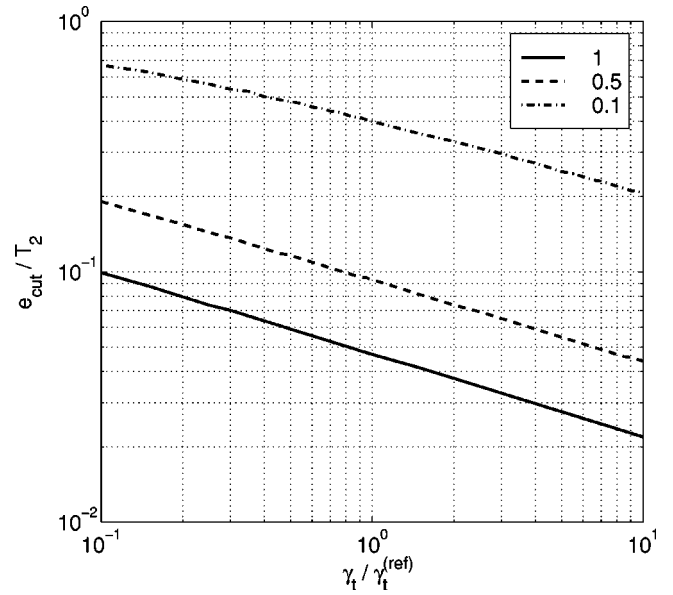


FIG. 8. These curves correspond to the curves in Figs. 5–7, showing the ratio of the RF cut to the temperature of atoms injected into the trap, e_{cut}/T_2 , as a function of the transfer rate γ_t . Along each of these curves, $\rho_0=2.612$.

background gas, as well as inelastic three-body collisions. Our model of the loading of atoms into the magnetic trap treats two idealizations of transferring atoms from a separate MOT; either an adiabatic or a sudden transfer. The description of the kinetic evolution to steady state assumes a truncated Boltzmann form for the nonequilibrium distribution $f(e,t)$, reducing the problem to that of solving coupled rate equations for the total number $N(t)$ and total energy $E(t)$ of the gas. Our calculations show that it is possible to achieve a steady-state condensation using optimistic values of the relevant physical parameters.

We have shown several results of numerical solutions of the rate equations in Eq. (12) and Eq. (13). First, we addressed the build-up time for steady state to occur and determined that an upper limit on the build-up time is given by the background loss lifetime τ_{bl} . If three-body losses are dominating due to a high density, then the build-up time will be much shorter than this. We next looked at how the steady-state value of the peak phase space density ρ_0 depends on the magnetic trap frequency ω_2 and the RF cut e_{cut} . We found that in the adiabatic case, one can gain a large increase in the total number in steady state N_{ss} by loosening the magnetic trap, while only losing a small amount in ρ_0 . This is not true for a sudden transfer. Finally, we looked at how one must vary the transfer rate γ_t and the MOT temperature T_1 in order to reach $\rho_0=2.612$. We found that ρ_0 depends more critically on T_1 than γ_t . Also, it was shown that one must try much harder to reach the critical point while achieving a large N_{ss} in the sudden case compared to the adiabatic case.

There are several shortcomings of our model which might be improved, however we believe that the present calculations are qualitatively correct and are sufficient for experimental guidance. An obvious extension to our model would be to include the effect of the growth of the condensate which will make the evaporation more efficient but at the same time increasing three-body losses due to the increase in

density in the center of the trap [4,23–25]. Another improvement would be to construct a more accurate model of the transfer process by understanding the relationship between T_1 , ω_1 , and γ_t , since these cannot be varied independently in an experiment. Alternatively, one could construct a model of the loading procedure based on an entirely different experimental method than that described in [19,20,11].

ACKNOWLEDGMENTS

J. Williams and M. Holland appreciated the hospitality of the Institute of Theoretical Physics at the University of Innsbruck during the earlier stages of this work. They thank Peter Zoller and Dieter Jaksch for helpful discussions. This work was supported by the National Science Foundation.

-
- [1] O. Luiten, M. Reynolds, and J. Walraven, *Phys. Rev. A* **53**, 382 (1996).
- [2] W. Ketterle and N. J. V. Druten, in *Advances in Atomic, Molecular, and Optical Physics, Vol. 37* (Academic Press, New York, 1996), p. 181.
- [3] M. Holland, J. Williams, K. Coakley, and J. Cooper, *Quantum Semiclass. Opt.* **8**, 571 (1996).
- [4] M. Holland, J. Williams, and J. Cooper, *Phys. Rev. A* **55**, 3670 (1997).
- [5] C. A. Sackett, C. C. Bradley, and R. G. Hulet, *Phys. Rev. A* **55**, 3797 (1997).
- [6] K. Berg-Sørensen, *Phys. Rev. A* **55**, 1281 (1997).
- [7] M. H. Anderson *et al.*, *Science* **269**, 198 (1995).
- [8] C. Bradley, C. A. Sackett, J. J. Tollett, and R. G. Hulet, *Phys. Rev. Lett.* **75**, 1687 (1995).
- [9] K. B. Davis *et al.*, *Phys. Rev. Lett.* **75**, 3969 (1995).
- [10] M.-O. Mewes *et al.*, *Phys. Rev. Lett.* **77**, 416 (1996).
- [11] C. J. Myatt *et al.*, *Phys. Rev. Lett.* **78**, 586 (1997).
- [12] In addition to the above citations, three other groups have reported observations of Bose-Einstein condensation using the technique of evaporative cooling on a cold atomic vapor.
- [13] M. O. Mewes *et al.*, *Phys. Rev. Lett.* **78**, 582 (1997).
- [14] M. Holland *et al.*, *Phys. Rev. A* **54**, R1757 (1996).
- [15] H. Wiseman, A. Martins, and D. Walls, *Quantum Semiclass. Opt.* **8**, 737 (1996).
- [16] R. J. Ballagh, K. Burnett, and T. F. Scott, *Phys. Rev. Lett.* **78**, 1607 (1997).
- [17] J. J. Hope, *Phys. Rev. A* **55**, R2531 (1997).
- [18] W. Ketterle and H.-J. Miesner, *Phys. Rev. A* **56**, 3291 (1997).
- [19] E. Cornell, C. Monroe, and C. Wieman, *Phys. Rev. Lett.* **67**, 2439 (1991).
- [20] C. J. Myatt *et al.*, *Opt. Lett.* **21**, 290 (1996).
- [21] C. G. Townsend *et al.*, *Phys. Rev. A* **52**, 1423 (1995).
- [22] E. A. Burt *et al.*, *Phys. Rev. Lett.* **79**, 337 (1997).
- [23] D. Jaksch, C. W. Gardiner, and P. Zoller, *Phys. Rev. A* **56**, 575 (1997).
- [24] C. W. Gardiner, P. Zoller, R. J. Ballagh, and M. J. Davis, *Phys. Rev. Lett.* **79**, 1793 (1997).
- [25] C. W. Gardiner and P. Zoller, *Phys. Rev. A* (to be published).